Article ID: 1006-8775(2019) 02-0257-12

THE IMPACT OF MOUNTAIN TO BASIN WINDS ON THE DIURNAL VARIATION IN FOG OVER THE SICHUAN BASIN, CHINA

ZHANG Fu-ying (张福颖)[1], LIU Hai-wen (刘海文)[2], ZHU Yu-xiang (朱玉祥)[3], ZHAO Liang (赵 亮)[4], DUAN Bo-long (段伯隆)[5], FU Ning (傅 宁)[2]

(1. Nanjing University of Information Science & Technology, Nanjing 210044 China; 2. Department of Aviation Meteorology, Civil Aviation University of China, Tianjin 300300 China; 3. CMA Training Center, China Meteorological Administration, Beijing 100081 China; 4. LASG, Institute of Atmospheric Physics, Chinese Academy of Sciences, Beijing 100029 China; 5. Lanzhou Central Meteorological Observatory, Lanzhou 730020 China)

Abstract: There is an increased demand for the accurate prediction of fog events in the Sichuan Basin (SCB) using numerical methods. A dense fog event that occurred over the SCB on 22 December 2016 was investigated. The results show that this dense fog event was influenced by the southwest of a low pressure with a weak horizontal pressure gradient and high relative humidity. This fog event showed typical diurnal variations. The fog began to form at 1800 UTC on 21 December 2016 (0200 local standard time on 22 December 2016) and dissipated at 0600 UTC on 22 December 2016 (1400 local standard time on 22 December 2016). The Weather Research and Forecasting model was able to partially reproduce the main features of this fog event and the diurnal variation in the local mountain to basin winds. The simulated horizontal visibility and liquid water content were used to characterize the fog. The mountain to basin winds had an important role in the diurnal variation of the fog event. The positive feedback mechanism between the fog and mountain to basin winds was good for the formation and maintain of the fog during the night. During the day, the mountain to basin wind displayed a transition from downslope flows to upslope flows. Water vapor evaporated easily from the warm, strong upslope winds, which resulted in the dissipation of fog during the day. The topography surrounding the SCB favored the lifting and condensation of air parcels in the lower troposphere as a result of the low height of the lifting condensation level.

Key words: mountain to basin winds; fog events; weather research and forecasting simulations; Tibetan Plateau

CLC number: P425.41 **Document code:** A

doi: 10.16555/j.1006-8775.2019.02.011

1 INTRODUCTION

The Sichuan Basin (SCB) in southwestern China is located to the east of the Tibetan Plateau, north of the Yunnan-Guizhou Plateau, west of the Wu Mountain range and south of the Daba Mountains (Qian et al.[1]). With this unique topography, the SCB is prone to frequent heavy fog events. Fog is a complex atmospheric phenomenon and can cause problems for both traffic (Duynkerke[2]) and human health (Nemery et al.[3]), resulting in losses to the local economy (Niu et al.[4]). The adverse effects of fog on aviation and marine and land transportation are comparable with the effects of tornadoes, winter storms or hurricanes (Gultepe and Milbrandt[5]).

The physical mechanisms for the formation of fog have been studied for more than a century (Gultepe et al.[6]). Pioneering research on fog, especially sea fog, can be traced back to the work of Taylor [7]. The formation of fog can be summarized as three primary processes: Cooling, moistening and the vertical mixing of air parcels with different temperatures and humidity[2]. Croft reported that clear skies caused by large-scale subsidence and light winds favor the formation of radiation fog [8]. Deng et al. detected daytime fog in the south of China using the current fog detection method[9]. Some invetstigators also discovered the microstructure of fog (Zhang et al.[10]; Fei et al.[11]). Zhang and Niu studied the transformation of haze to fog[12].

Work on numerical modeling of the onset and development of fog has a long history (Van Der Velde et al.[13]). Fisher and Caplan constructed a numerical model for forecasting fog and low stratus clouds[14]. Since then, a variety of models have been used to simulate fog-related events (Baker et al.[15]; Pagwski et al.[16]; Shi et al.[17]; Zhou and Du [18]; Román-Cascón et al.[19]; Hu et al.[20]; Huang et al.[21]; Müller [22]). As an advanced mesoscale numerical weather prediction system, the Weather Research and Forecasting (WRF)

Received 2018-03-02; **Revised** 2018-12-15; **Accepted** 2019-05-15

Foundation item: Applied Basic Research Programs of the Science and Technology Department of Sichuan Province (2015JY0109); State Key Program of National Natural Science of China (91337215, 41475051); Starting Foundation of the Civil Aviation University of China (2016QD05X)

Biography: LIU Hai-wen, Ph. D., Professor, primarily undertaking aviation weather and research on climate change.

Corresponding author: LIU Hai-wen, e-mail: hwliu@lasg.iap.ac.cn

model has been successfully used to simulate fog[13, 18, 22]) and has shown potential in simulating sea fog (Gao et al.[23]). However, numerical weather prediction (NWP) models have relatively low skill in forecasting both the onset and development of fog (Gultepe and Milbrandt[5]; Steeneveld et al.[24]). Hu et al. investigated the sensitivity of fog to different initial conditions using an ensemble-based method[20].

Located in the east of the Tibetan Plateau, the SCB (Fig. 1) is often influenced by mountain to valley winds (Huang et al. [25]). Mountain and plain winds are produced by the thermal contrast between the air over the mountains and the air at the same level over the plains (De Wekker et al.[26]). A large-scale circulation of mountain and plain winds (Doran and Zhong[27]; Bossert and Cotton [28]; Bossert [29]) feeds low-level air into the mountain ranges during the day and out of the mountain ranges during the night, with the upper branch of the circulation blowing in an opposite direction to the low-level flows. Abrupt changes in wind direction within small vertical distances above the valley are the most significant features of mountain to valley wind systems (Buettneer and Thyer[30]; Moore et al.[31]).

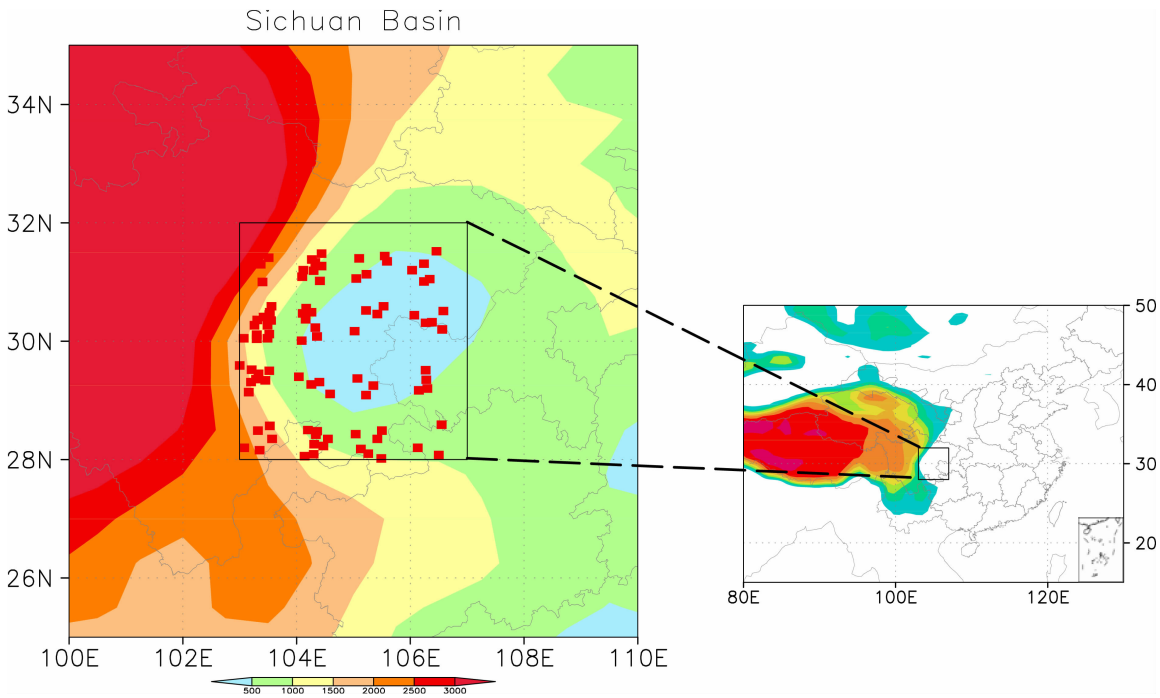

Figure 1. Location of the 109 weather stations (red squares) in the SCB and the location of the SCB (black rectangle). The shading represents the surface elevation of the surrounding the SCB in meters.

Mountain to valley winds not only produce a wide spectrum of weather phenomenon, ranging from the regional to global scale (Gao et al.[32]; Reiter[33]; Kuo and Anthes [34]), but also can move pollutants in and out of valleys and transport them to higher or lower elevations through diurnal variations in the downslope and upslope flows[31]. Mountain to valley wind systems have a variety of practical implications for the transport and diffusion of local weather and air pollution[26].

Numerical models are also used to simulate mountain to valley winds (Chow et al.[35]; Weissmann et al.[36]). De Wekker et al. developed a mesoscale model to examine the diurnal variation in temperature in a basin and the thermally driven plain to basin winds through a variety of simulations with different basin geometries[26]. To measure the diurnal cycle of mountain to valley winds, a dry three-dimensional mesoscale model was used in the southern San Joaquin Valley, California (USA) on a summer day [31]. To study large-scale thermally driven wind systems in mountainous areas, previous investigators have referred to mountain to plain wind systems in different ways[26]. In this paper, we refer to the thermally driven wind systems between the Tibetan Plateau and the SCB as mountain to basin winds.

The mountain to basin flow may play an important part in the transport of air pollutants over complex terrain, but has not been studied as extensively as other wind systems in complex terrain (De Wekker et al.[26]; Wilson and Barros [37]). Unlike the work of Müller et al.[38] and Cuxart and Jiménez [39], high-resolution NWP models provide reasonable results because the problem in complex terrains with closed basins is confined to the basin. However, few studies have explored the influence of mountain to basin winds on the diurnal variations of fog over SCB.

The purpose of this paper is to evaluate: (1) the ability of the WRF model to simulate fog in this region

of unique topography; (2) the ability of the WRF output products to simulate the diurnal variation in both fog and mountain to basin winds; and (3) the possible mechanisms of the impact of mountain to basin winds on the diurnal variation in fog. This paper is organized as follows. Section 2 describes the datasets and configurations of the WRF simulations. Section 3 uses model simulations to examine the mountain to basin winds and their impact on the diurnal variations of fog. Section 4 summarizes the main findings and discusses the results.

2 CASE OVERVIEW

2.1 *Episodes and observations*

Datasets of the six-hourly visibility measured by surface meteorological observations were provided by the National Meteorological Information Center of the China Meteorological Administration. Fig. 1 shows the location of the 109 stations within the region used to represent the SCB (28° –32° N, 103° –107° E). The NOAA definition of fog is a collection of suspended water droplets or ice crystals near the Earth's surface that leads to a reduction in the horizontal visibility to <1 km [40]. Based on this definition, Fig. 2 shows the spatial distribution of fog over the SCB based on the visibility datasets provided by the China Meteorological Administration. At 1800 UTC on 21 December 2016 (0200 local standard time on 22 December 2016), fog was observed by a small number of weather stations and affected a large area of the SCB six hours later. This fog event caused Chengdu Shuangliu International Airport to shut down and more than 100 flights were grounded. By 0600 UTC on 22 December 2016, the fog had dissipated over most parts of SCB. This fog event showed a distinct diurnal variation. The fog began to form at 1800 UTC on 21 December 2016 and dissipated at 0600 UTC on 22 December 2016.

The National Centers for Environmental Prediction Final operational global analysis six-hourly dataset on a 1.0°×1.0° grid was used for synoptic analysis based on the heights at 500 hPa and the sea-level pressure, surface winds and relative humidity (Fig. 3). Fig. 3a shows a deep trough and a ridge at mid-high attitudes. The trough stretched from Lake Baikal to the Altai Mountains. There was another trough at mid-low attitudes with a southwesterly orientation from the northern SCB to the Yunnan–Guizhou Plateau and a dominant long wavelength ridge from northeastern China to the south of China. This long wavelength ridge obstructed rapid movement of the deep trough at 500 hPa. The SCB was influenced by a relatively weak easterly flow (Fig. 3c). At 0600 UTC (Fig. 3b and 3d), the overall weather situation was unchanged from the previous six hours. The fog began to dissipate during this period, but low-level jets had no direct influence on the formation and dissipation of the fog.

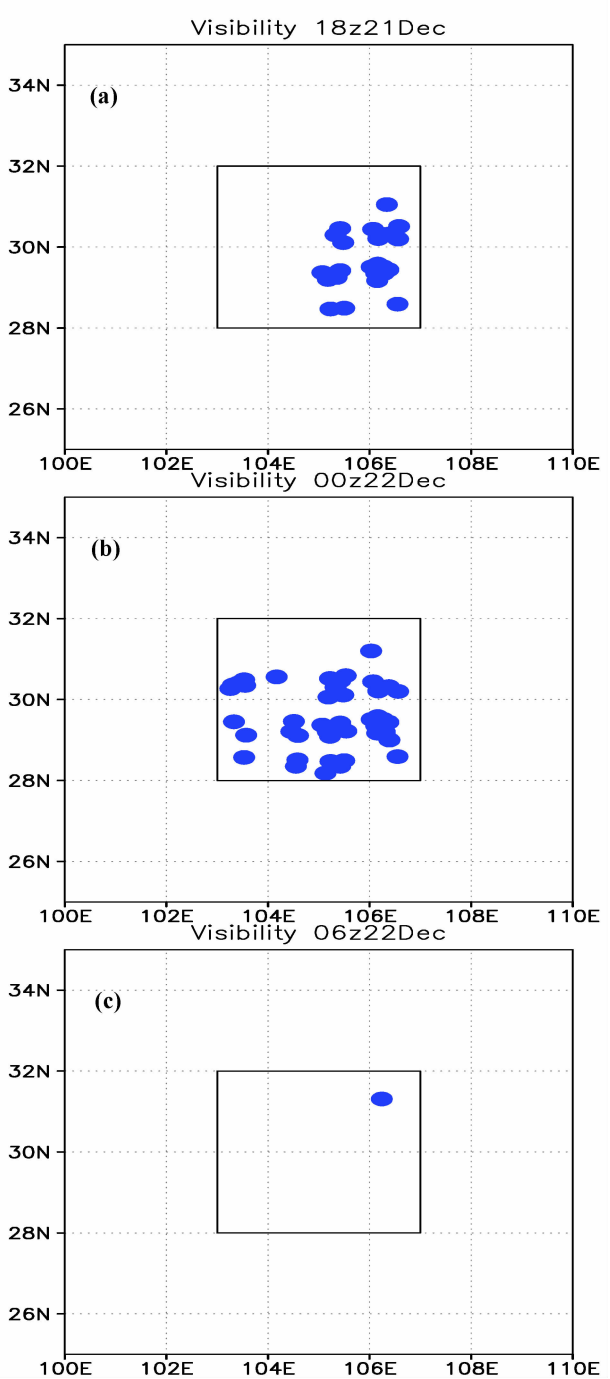

Figure 2. Spatial distribution of the horizontal visibility over the SCB at (a) 1800 UTC on 21 December 2016, (b) 0000 UTC on 22 December 2016, (c) 0600 UTC on 22 December 2016. The blue dots show when the horizontal visibility was <1 km. The black rectangle shows the location of the SCB.

The SCB was dominated at the surface by the southwest of the low pressure with a weak horizontal pressure gradient and moist air. Unlike in other areas, such as the north of China, there was no need for southerly and easterly winds to supply moisture to the SCB. The high levels of moisture led to a relative humidity >80% over the SCB at 0000 UTC on 22 December, 2016. The abundant moisture and weak wind

conditions were suitable for the formation and maintenance of fog. However, the low pressure moved northeastward to the Sea of Japan six hours later and the SCB was controlled by a small area of low pressure. The fog dissipated at this time.

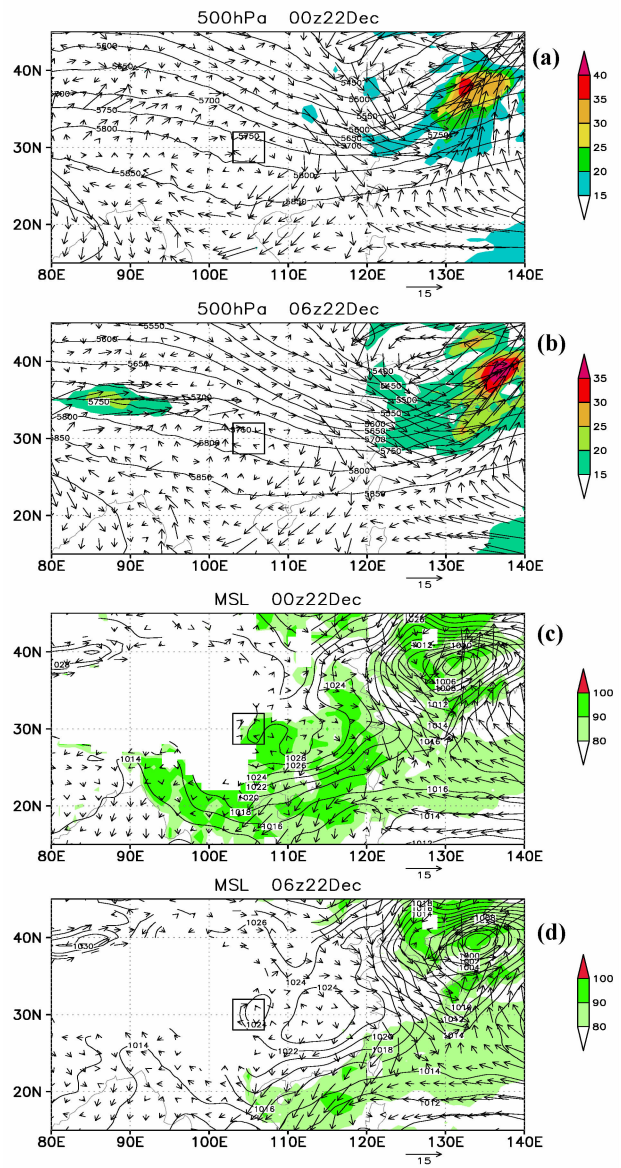

Figure 3. Synoptic review of the fog event at (a, c) 0000 UTC on 22 December 2016 and (b, d) 0600 UTC on 22 December 2016. (a, b) 500 hPa geopotential height, 850 hPa wind vectors (magnitudes ⩾12 m/s are shaded). (c, d) Sea-level pressure (contours every 2 hPa), 10 m winds and relative humidity (shading). The black rectangle indicates the location of the SCB and the region with no data is the Tibetan Plateau.

Figure 4 shows the measurements made at Xichong weather station (30.59°N, 105.53°E) at 0000 UTC on 22 December 2016. There was an inversion layer below about 925 hPa and the dew point temperature profile was close to the temperature profiles in the lower troposphere, suggesting that the atmosphere was nearly saturated. The vertical wind shear was very obvious from 1,000 hPa to 500 hPa. Light southerly and southeasterly winds were observed from the surface to 900 hPa, whereas the winds above 600 hPa were northwesterly. Taylor stressed that the wind shear play important roles for the fog formation by the vertical transport of air properties [41]. Radiative cooling and mixing of air parcels with different temperatures and humidities was generalized into two primary processes (Pagowski et al. [42]): The low height of the lifting condensation level (LCL) and the vertical wind shear favored the formation of fog.

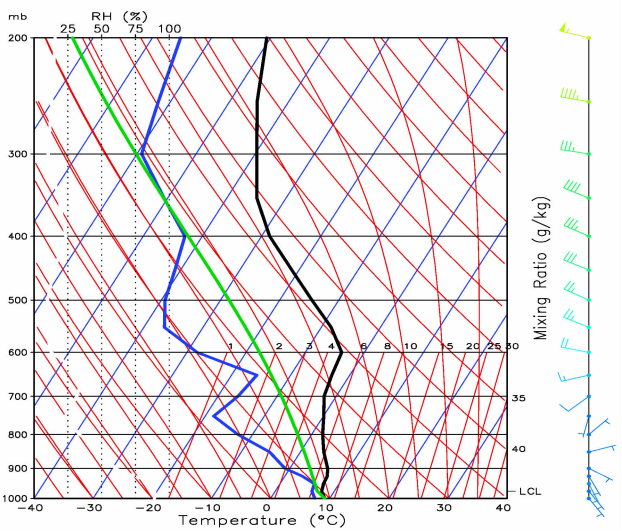

Figure 4. Skew *T*-log*p* diagrams of measurements taken at Xichong weather station (30.59°N, 105.53°E) at 0000 UTC on 22 December 2016. Atmospheric measurements showing the temperature (black), parcel trace line (green), dew point temperature (blue) in a skew *T*-log*p* diagram.

2.2 *Experimental design*

The WRF model version 3.7.1 (Skamarock[43]) was used in this study to examine the mountain to basin winds. Three nesting domains with horizontal resolutions of 27, 9 and 3 km, respectively, were implemented (Fig. 5). The coarse domain (D01) was centered at (32.8°N, 102.5°E) and consisted of 191×171 grids spanning the whole of eastern Asia, giving a horizontal resolution of 27 km for the study of the synoptic-scale environment. The nested grid (D02) consisted of 277 ×247 grids covering eastern China, including the SCB, with a horizontal resolution of 9 km. The inner domain consisted of 457×370 grids covering the region where the fog event occurred. A one-way interaction was used in all domains. The model top was at 50 hPa and there were 50 vertical levels with 15 levels below 1 km. Because vegetation has an important influence on the formation of fog [2], we used the 500 m land use data for the year 2000 (Zhang et al. [44]) for D03. The WRF single-moment six-class microphysics scheme (Hong and Lim[45]), the Rapid Radiative Transfer Model longwave radiation scheme (Mlawer et al.[46]), the Dudhia shortwave radiation scheme (Dudhia[47]), and the Quasi-Normal Scale Elimination (QNSE) planetary boundary layer and surface layer schemes (Sukoriansky

et al. [48]) were used for parameterization in the simulation. The Kain-Fritsch cumulus scheme (Kain[49]) was used only for D01 and D02.

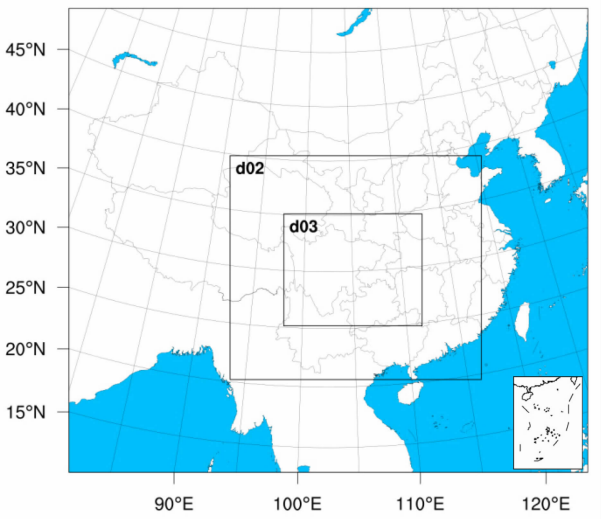

Figure 5. Configuration of the nested model domains.

The initial and boundary conditions were derived from the National Centers for Environmental Prediction Final operational global analysis dataset with 1° ×1° grids every six hours. The simulation was initialized at 1200 UTC on 21 December 2016 and integrated until 1200 UTC on 22 December 2016 with the initial and boundary conditions provided by the six-hourly National Centers for Environmental Prediction Final data. In addition to the control simulation using the default terrain, a no terrain variability experiment was conducted between the mountain and basin. All the high terrains related to mountains surrounding the SCB in the model were flattened to 500 m to measure the diurnal variations in the mountain to basin winds. All the modeling set-ups, such as the integration time and domain size, were kept the same as in the previous WRF simulation.

3 RESULTS

3.1 *Ability of the WRF model to simulate fog*

Horizontal visibility is a significant variable in identifying grades of fog. It is defined as the greatest distance at which selected objects can be seen and identified. The horizontal visibility in the WRF model can be calculated with an algorithm developed by Kunkel [50] and Stoelinga and Warner [51] based on the extinction coefficients of various hydrometeors:

$$\mathrm{Vis}=\frac{-\ln(0.02)}{\beta} \quad (1)$$

where the extinction coefficient β includes the effects due to cloud water, cloud ice, snow and rain water. This method has been widely used in fog simulations (Gao et al.[23]; Fu et al.[52]). The area where the visibility was <1 km according to equation (1) was much smaller in Fig. 6 than in Fig. 3, and the WRF model was able to simulate the diurnal variations in fog over the SCB. At 0000 UTC on 22 December 2016, the coverage of fog was simulated for the SCB, although there was some bias (visibility <1000 m) compared with the observations (Fig. 2). The results of the simulation indicated that the fog had dissipated by 0600 UTC on 22 December 2016 (not shown).

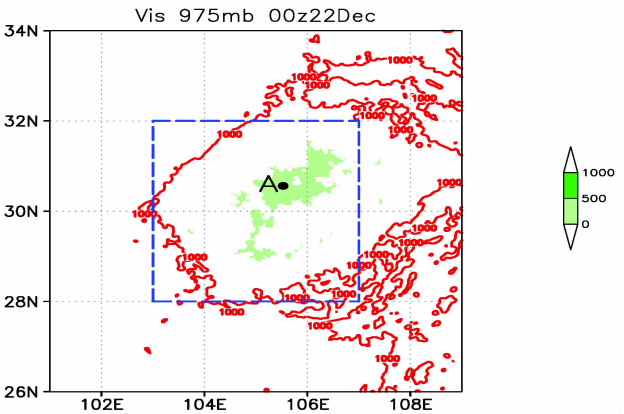

Figure 6. Simulated surface visibility (m) at 975 hPa from D03 at 0000 UTC on 22 December 2016. The letter A denotes the location of Xichong weather station (30.59°N, 105.53°E) and the blue rectangle denotes the location of the SCB.

Liquid water content is the most important factor for the fog formation and development (Li et al.[53]). Fig. 7 shows the distribution of the LWC which was consistent with the visibility and also showed a diurnal variation. At 0000 UTC on 22 December 2016, the maximum LWC was mainly located in the SCB, although wide areas of LWC were observed in the northeast of the SCB during the dissipation of the fog at 0600 UTC on 22 December 2016.

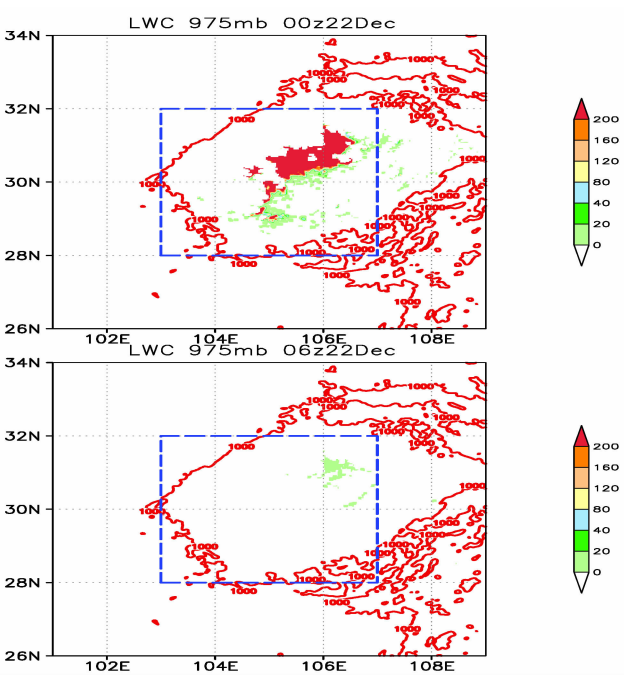

Figure 7. Simulated liquid water content (LWC) (0.001 g/m^3) at 975 hPa from D03 at (a) 0000 UTC and (b) 0600 UTC on 22 December 2016. Contours show the topography in meters. The blue rectangle denotes the location of the SCB.

3.2 *Performance of the WRF model in simulating the mountain to basin winds*

To investigate the diurnal variation in the mountain to basin winds, Fig. 8 shows the simulated wind at 10 m and the relative humidity at 2 m from D03. The diurnal variation in the mountain to basin winds and the relative humidity were simulated well by the WRF model. At 0000 UTC on 22 December 2016, the SCB was dominated by downslope winds from the mountains into the SCB and the relative humidity was >80% in the west of the SCB. The downslope winds converged in the SCB. As a continuous fluid of the atmosphere, the converged surface flow favored the flow of downslope winds from the surrounding mountains into the SCB during the night. This downslope winds with a high relative humidity favored the formation of fog after cooling. By 0600 UTC on 22 December 2016, the downslope winds had changed to upslope winds and the relative humidity was <80% . The velocity of the upslope flows was greater than that of the downslope flows. The stronger winds and lower relative humidity favored the dissipation of the fog. This result helps to explain the diurnal variations in fog.

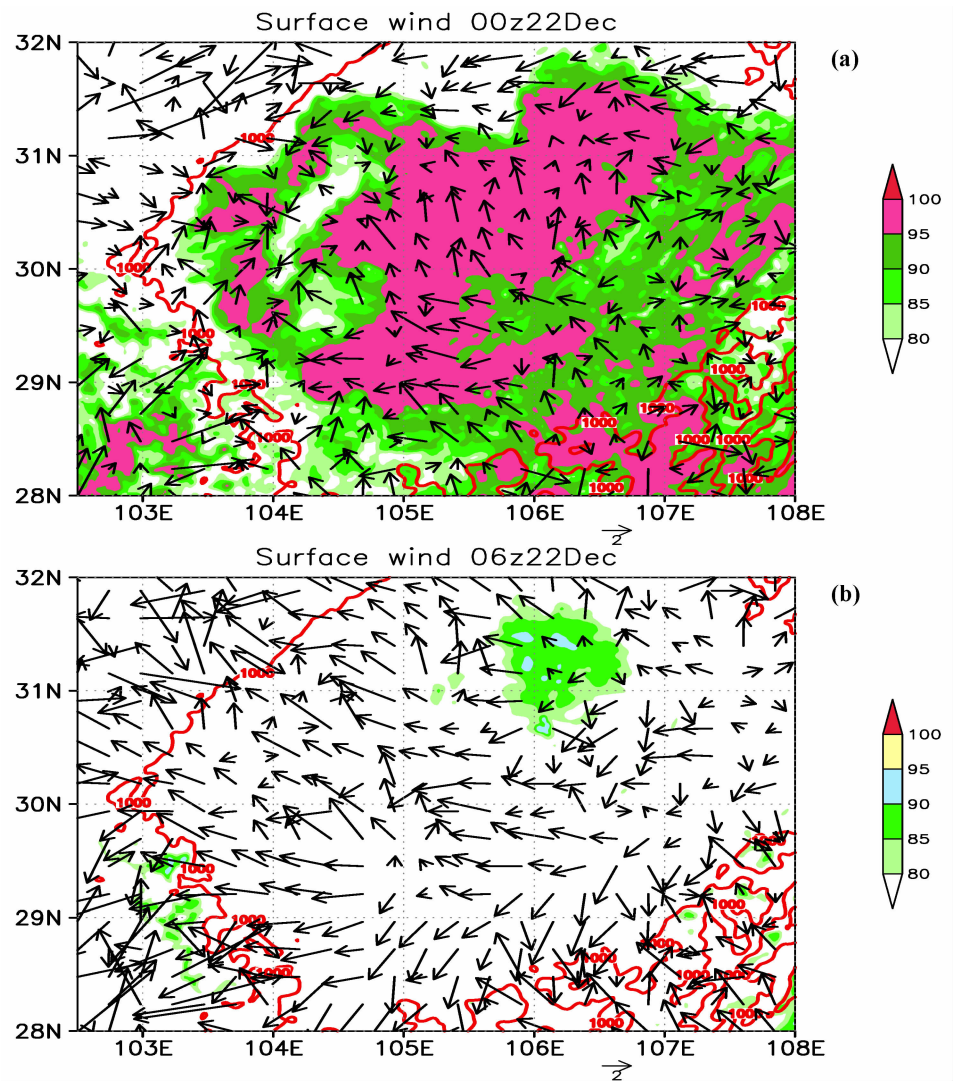

Figure 8. Simulated surface horizontal wind (m/s) and relative humidity from D03 at (a) 0000 UTC and (b) 0600 UTC on 22 December 2016. Contours represent the topography in meters.

Mountain to basin winds, as the phenomana of in the lower layers of the atmosphere, the winds at 900 hPa direction between the Tibetan Plateau and the SCB were no longer reversed at 0000 UTC 12 and 0600 UTC 22 on December 2016 (not shown). The weather map at 900 hPa shows that anticyclone flows and an anticyclone center were observed in the SCB.

3.3 *Possible impacts of the mountain to basin winds on the diurnal variations in fog*

Cold air trapped in valleys or large basins and the associated cooling is a necessary condition for persistent fog (Zhou and Ferrier [54]). To investigate the possible influence of the mountain to basin winds on the diurnal variation in fog, Fig. 9 shows the simulated surface horizontal wind and air temperature from D03 at 0000 UTC and 0600 UTC on 22 December 2016. The

subsiding downslope winds carried cooling air of near surface moist flow resulting from an adiabatic expansion into the SCB. Due to the law of conservation of mass, the converged downslop winds within the SCB prompted the warm and wet air to lift up (Fig. 9a). The uplifting warm and wet air was favorable to the formation and development of temperature inversion layer and fog [4]. Meanwhile, the stability of lower atmospheric level over SB favored downslope winds to move into the SCB. So the positive feedback mechanism between the fog and mountain to basin winds was formed. However, during the day, the mountain to basin winds changed from downslope flows to upslope flows (Fig. 9b). Water vapor evaporated from the warmer and stronger upslope winds, resulting in the dissipation of the fog.

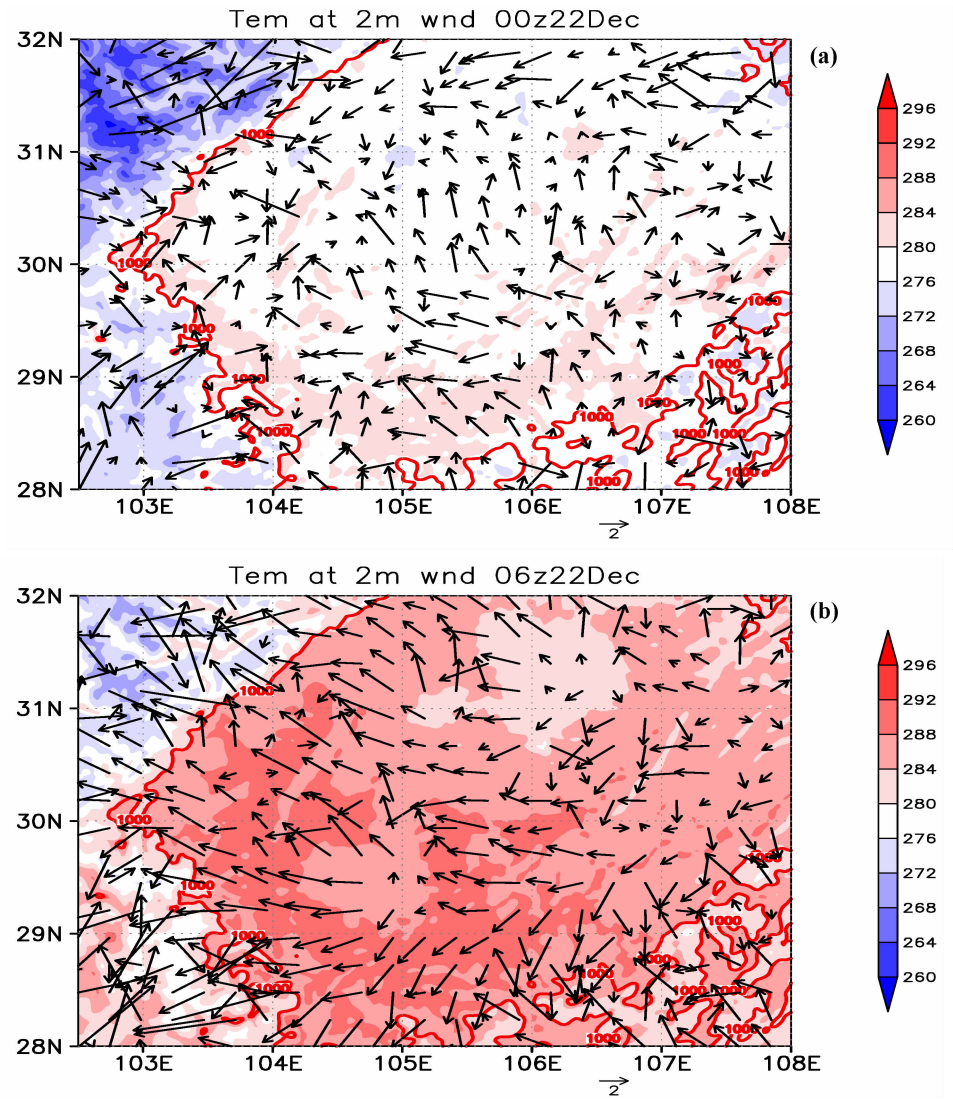

Figure 9. Simulated surface horizontal winds (m/s) and air temperature (K) from D03 at (a) 0000 UTC and (b) 0600 UTC on 22 December 2016. Shading represents air temperature.

Mountain to basin winds are essentially produced by the thermal contrast between air over the mountains and air at the same level over the plains [26]. To further evaluate the impact of mountain to basin winds on the diurnal variation in the occurrence of fog, a no terrain variability experiment was conducted. The converged flow over the SCB seen in Fig. 8 is no longer observed in Fig. 10 and the wind between the Tibetan Plateau and SCB was dominated by a synoptic-scale flow (Fig. 10). The SCB was influenced by the northwesterly flow from behind the area of low pressure located in the Sea of Japan (Fig. 3c). By 0600 UTC on 22 December 2016, the direction of the winds between the Tibetan Plateau and SCB did not show a diurnal variation, although there was one in the relative humidity between the Tibetan Plateau and SCB in the west of the SCB. The distribution of air temperature was different from the control experiment in Fig. 11. No thermal contrast is seen in Fig. 11 between the air over the mountains and the air over the SCB. The air temperature gradually increased from the northeast to the southwest.

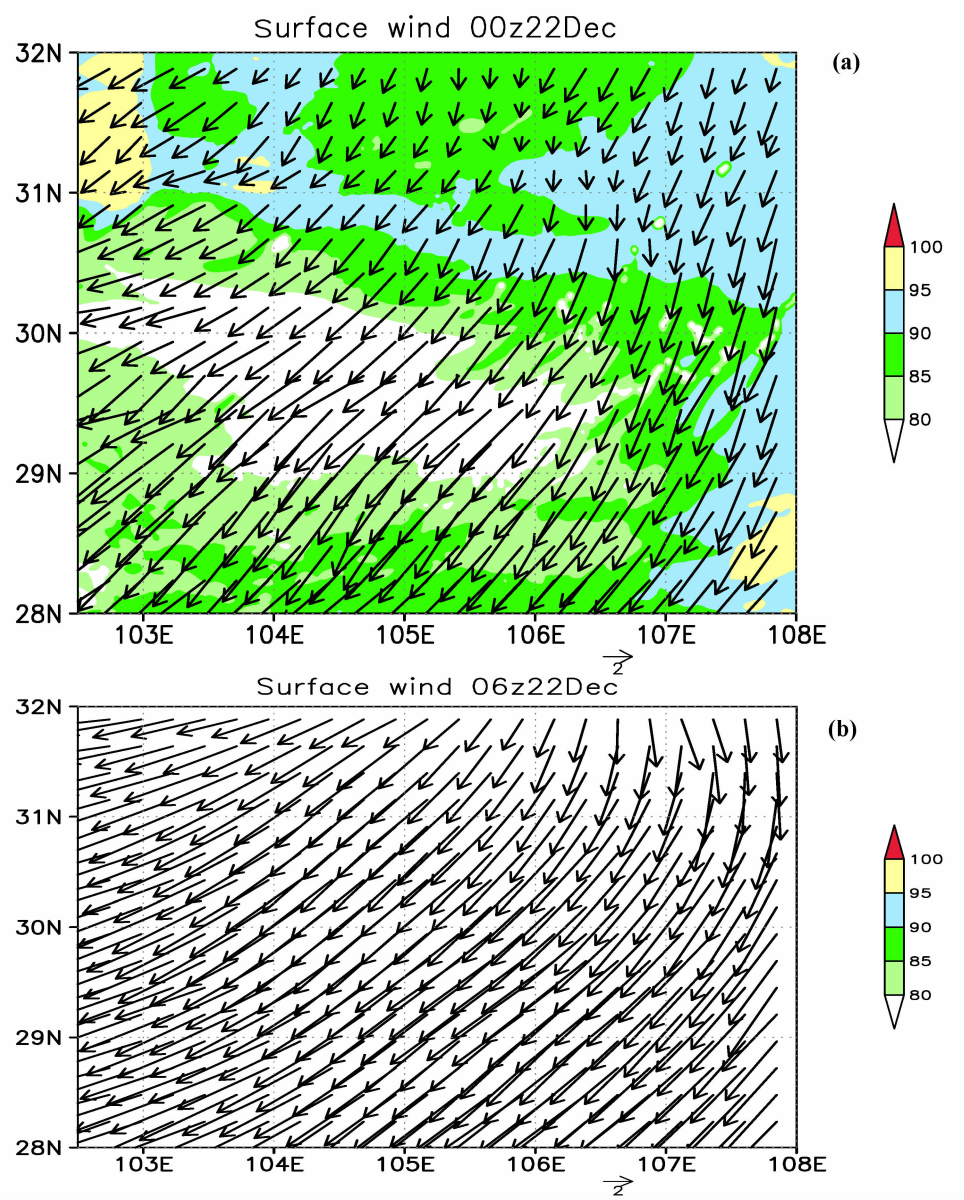

Figure 10. Simulated surface horizontal wind (m/s) and relative humidity from the no terrain variability experiment at (a) 0000 UTC and (b) 0600 UTC on 22 December 2016.

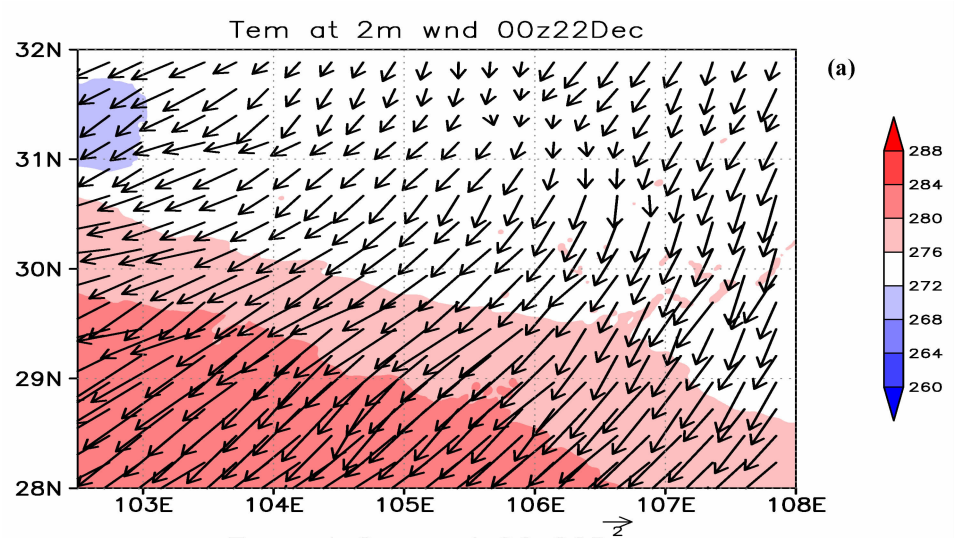

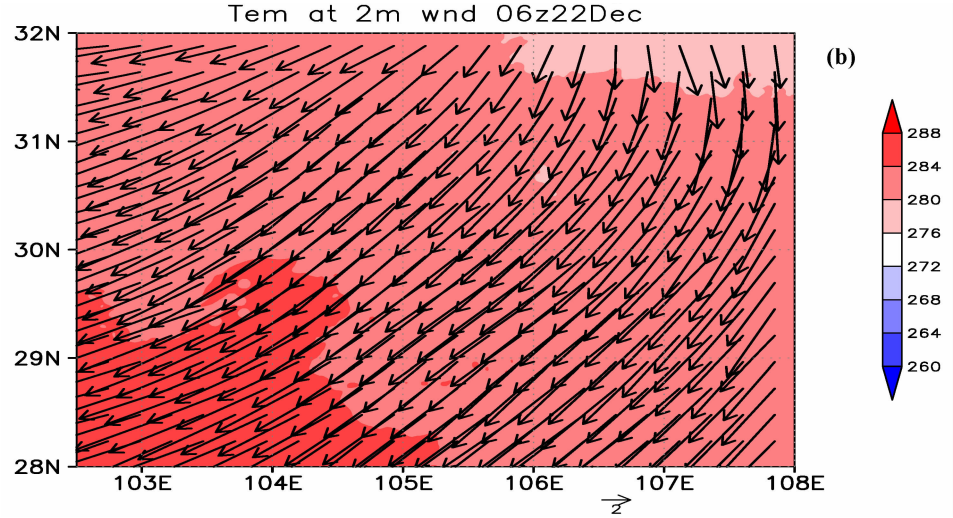

Figure 11. Simulated surface horizontal winds (m/s) and air temperature (K) from the no terrain variability experiment 3 at (a) 0000 UTC and (b) 0600 UTC on 22 December 2016. Shading represents air temperature.

The terrain surrounding the SCB had a significant effect on the distribution of the LWC (Fig. 12). The LWC was mainly located in the southwest of the SCB, suggesting that fog was unable to form within the SCB. The LWC showed diurnal variations, but the distribution of the LWC was different from that in the control test. The inverse inversion layer below 925 hPa and warm advection between 500 and 900 hPa can be seen in the skew T-log$p$ diagrams for the Xichong weather station (Fig. 13); however, the height of the LCL is higher in Fig. 13 than in Fig. 4, suggesting that the topography has an important role in lifting the air parcel. The difference between the temperature and dew point was greater than the observed value. The higher height of the LCL in the no terrain variability experiment did not favor the formation of surface fog.

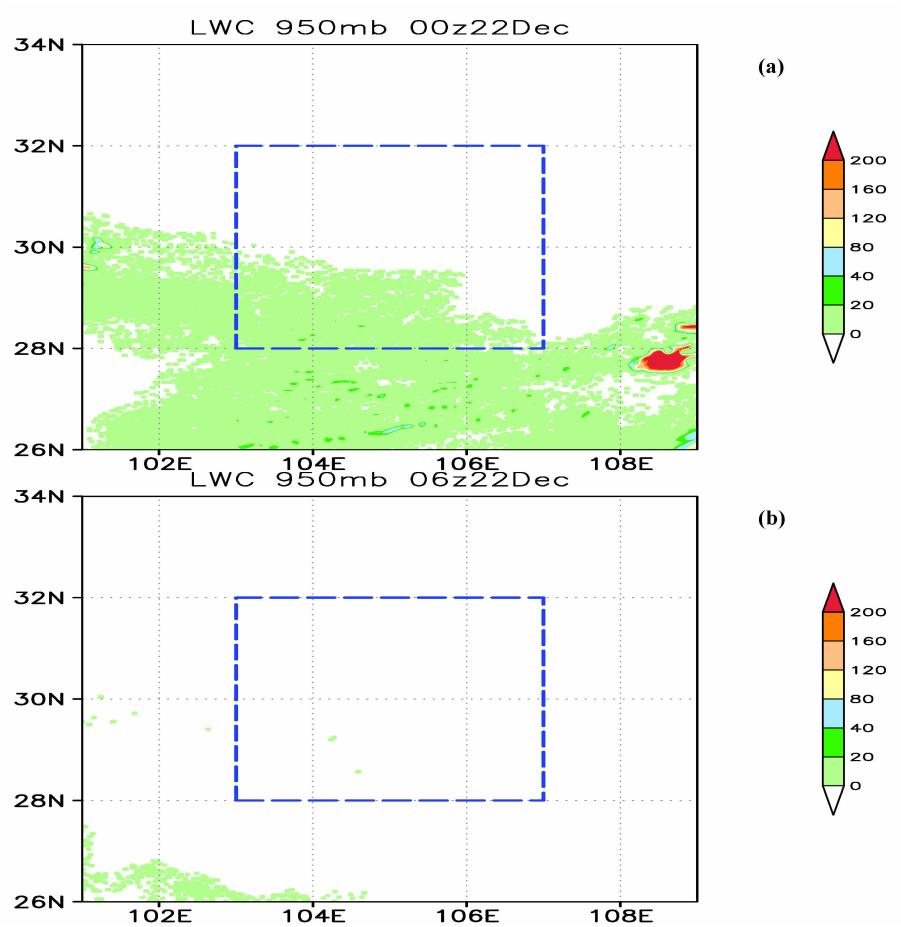

Figure 12. Simulated liquid water content (LWC) (0.001 g/m^3) at 975 hPa from the no terrain variability experiment at (a) 0000 UTC and (b) 0600 UTC on 22 December 2016.

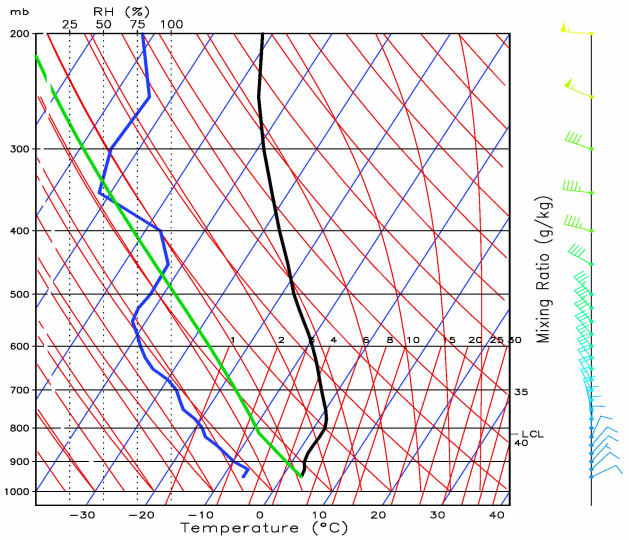

Figure 13. Skew *T*-log*p* diagrams of soundings taken at A (Xichong weather station, 30.59° N, 105.53° E) of Fig. 6 at 0000 UTC on 22 December 2016 in the no terrain variability experiment. Atmospheric measurements showing the temperature (black), parcel trace line (green), dew point temperature (blue) in a skew *T*-log*p* diagram.

4 CONCLUSIONS

It is difficult to use NWP to predict the occurrence of fog in this region as a result of the unique topography. We examined the relationship between a fog event and the mountain to basin winds over the SCB and carried out an experiment where there was no difference except the terrain between the mountain and basin. The main conclusions of this study are as follows.

(1) Dominated by the southwest of low pressure with a weak horizontal pressure gradient and high relative humidity conditions, a dense fog event occurred over the SCB on 22 December 2016. This dense fog event showed a typical diurnal variation. It began to form at 1800 UTC on 21 December 2016 and dissipated at 0600 UTC on 22 December 2016.

(2) The WRF model was able to simulate the horizontal visibility and the LWC, although the horizontal visibility and the LWC were smaller than the observed values. The horizontal visibility and LWC were significant variables in identifying the occurrence of fog in this case study.

(3) The WRF model was able to simulate the diurnal variation in the mountain to basin winds, which was a result of the topography surrounding the SCB. The converged surface flow favored the flow of downslope winds from the surrounding mountains into the SCB during the night. The mountain to basin winds were not observed in the no terrain variability experiment and the SCB was mainly influenced by synoptic-scale systems.

(4) The mountain to basin winds had an important effect on the diurnal variation of the fog. During the night, the mountain to basin winds caused the cold air to sink along the mountain slope and converged within the SCB, and made the warm and wet air lift up. The positive feedback mechanism between the fog and mountain to basin winds was good for the formation and maintain of the fog. However, during the day, the mountain to basin winds displayed a transition from downslope to upslope flows. The warm and strong upslope winds were prone to the evaporation of water vapor, which resulted in the dissipation of the fog. The topography surrounding the SCB favored lifting and condensation of the air parcel in the lower troposphere as a result of the lower height of the LCL.

REFERENCES:

[1] QIAN T, ZHAO P, ZHANG F, et al. Rainy-season precipitation over the Sichuan Basin and adjacent regions in southwestern China [J]. Mon Wea Rev, 2015, 143(1): 383-394.

[2] DUYNKERKE P G. Radiation Fog: A comparison of model simulation with the detailed observations [J]. Mon Wea Rev, 1991, 119(2): 324-341.

[3] NEMERY B, HOET P H, NEMMAR A. The meuse valley fog of 1930: An air pollution disaster [J]. Lancet, 2001, 357(9257): 704-708.

[4] NIU Sheng-jie, LU Chun-song, YU Hua-ying, et al. Fog research in China: An overview [J]. Adv Atmos Sci, 2010, 27(3): 639-662.

[5] GULTEPE I, MILBRANDT J A. Microphysical observations and mesoscale model simulation of a warm fog case during FRAM project [J]. J Pure Appl Geophys, 2007, 164(6-7): 1161-1178.

[6] GULTEPE I, TARDIF R, MICHAELIDES S C, et al. Fog research: A review of past achievements and future perspectives [J]. J Pure Appl Geophys, 2007, 164(6-7): 1121-1159.

[7] TAYLOR G I. The formation of fog and mist [J]. Quart J Roy Meteor Soc, 1917, 43(183): 241-268.

[8] CROFT P J. Encyclopedia of Atmospheric Sciences [M]. Manhattan: Academic Press, 2003: 777-792.

[9] DENG Yu-jiao, WANG Jie-chun, CAO Jing, et al. Detection of daytime fog in South China Sea using MODIS data [J]. J Trop Meteor, 2014, 20(4): 386-390.

[10] ZHANG Yue, FAN Shu-xian, ZHANG Shu-ting, et al. Microstructures and temporal variation characteristics during a sea fog event along the west coast of the Taiwan Strait [J]. J Trop Meteor, 2017, 23(2): 155-165.

[11] FEI Dong-dong, NIU Sheng-jie, YANG Jun. Analysis of the microphysical structure of radiation fog in Xuanen mountainous region of Hubei, China [J]. J Trop Meteor, 2017, 23(2): 177-190.

[12] ZHANG Shu-ting, NIU Sheng-jie. Haze-to-fog transformation during a long lasting, low visibility episode in Nanjing [J]. J Trop Meteor, 2016, 22(S1): 67-77.

[13] Van Der VELDE I R, STEENEVELD G J, SCHREUR B G J W, et al. Modeling and forecasting the onset and duration of severe radiation fog under frost conditions [J]. Mon Wea Rev, 2010, 138(11): 4237-4253.

[14] FISHER E L, CAPLAN P. An experiment in numerical prediction of fog and stratus [J]. J Atmos Sci,1963, 20 (5): 425-437.
[15] BAKER R, CRAMER J, PETERS J. Radiation fog: UPS airlines conceptual models and forecast methods [C] //Proc 10th conf on aviation, range and aerospace meteorology. Portland: Amer Meteor Soc, 2002: 154-159.
[16] PAGWSKI M, GULTEPE I, KING P. Analysis and modeling of an extremely dense fog event in Southern Ontario [J]. J Appl Meteor, 2004, 43(1): 3-16.
[17] SHI C, YANG J, QIU M, et al. Analysis of an extremely dense regional fog event in Eastern China using a mesoscale model [J]. Atmos Res, 2010, 95(4): 428-440.
[18] ZHOU B, DU J. Fog prediction from a multimodel mesoscale ensemble prediction system [J]. Wea Forecasting, 2010, 25(1): 303-322.
[19] ROMÁN-CASCÓN C, YAGÜE C, SASTRE M, et al. Observations and WRF simulations of fog events at the Spanish Northern Plateau [J]. Adv Sci Res, 2012, 8(1): 11-18.
[20] HU H, ZHANG Q, XIE B, et al. Predictability of an advection fog event over North China, Part I: Sensitivity to initial condition differences [J]. Mon Wea Rev, 2014, 142(5): 1803-1822.
[21] HUANG Hui-jun, ZHAN Guo-wei, LIU Chun-xia, et al. A case study of numerical simulation of sea fog on the southern China Coast [J]. J Trop Meteor, 2016, 22(4): 497-507.
[22] MÜLLER M D. Numerical simulation of fog and radiation in complex terrain [D]. Basel: University of Basel, 2006: 90.
[23] GAO Shan-dong, LIN Hang, SHEN Biao, et al. A heavy sea fog event over the Yellow Sea in March 2005: Analysis and numerical modeling [J]. Adv Atmos Sci, 2007, 24(1): 65-81.
[24] STEENEVELD G J, RONDA R J, HOLTSLAG A A M. The challenge of forecasting the onset and development of radiation fog using mesoscale atmospheric models [J]. Bound-Layer Meteor, 2015, 154(2): 265-289.
[25] HUANG H L, WANG C C, CHEN T J, et al. The role of diurnal solenoidal circulation on propagating rainfall episodes near the eastern Tibetan Plateau [J]. Mon Wea Rev, 2010, 138(7): 2975-2989.
[26] De WEKKER S F J, ZHONG S, FAST J D, et al. A numerical study of the thermally driven plain-to-basin wind over idealized basin topographies [J]. J Appl Meteor, 1998, 37(6): 606-622.
[27] DORAN J C, ZHONG S. Regional drainage flows in the Pacific Northwest [J]. Mon Wea Rev, 1994, 122 (6): 1158-1167.
[28] BOSSERT J E, COTTON W R. Regional-scale flows in mountainous terrain, Part I: A numerical and observational comparison [J]. Mon Wea Rev, 1994, 122 (7): 1449-1471.
[29] BOSSERT J E. An investigation of flow regimes affecting the Mexico City region [J]. J Appl Meteor, 1997, 36(2): 119-140.
[30] BUETTNEER K J K, THYER N. Valley winds in the Mount Rainier area [J]. Arch Meteor Geophys Bioklim, 1966, 14(2): 125-147.
[31] MOORE G E, DALY C, LIU K M. Modeling of mountain-valley wind fields in the southern San Joaquin valley, California [J]. J Appl Meteor, 1987, 26 (9): 1230-1242.
[32] GAO Y, TANG M, LUO S. Some aspects of recent research on the Qinghai-Xizang Plateau meteorology [J]. Bull Amer Meteor Soc, 1981, 62(1): 31-35.
[33] REITER E R. Thermal effects of the Tibetan Plateau on atmospheric circulation systems [C]//Proceedings of the first Sino-American workshop on mountain meteorology. Beijing, 1982 (in Chinese).
[34] KUO Y H, ANTHES R A. Mesoscale budgets of heat and moisture in a convective system over the central United States [J]. Mon Wea Rev, 1984, 112(8): 1482-1497.
[35] CHOW F K, WEIGEL A P, STREET R L, et al. High-resolution large-eddy simulations of flow in a steep Alpine valley, Part I: Methodology, verification, and sensitivity experiments [J]. J Appl Meteor Climatol, 2006, 45(1): 63-86.
[36] WEISSMANN M, BRAUN F J, GANTNER L, et al. The Alpine mountain-plain circulation: Airborne Doppler lidar measurements and numerical simulations [J]. Mon Wea Rev, 2005, 133(11): 3095-3109.
[37] WILSON A M, BARROS A P. Orographic land-atmosphere interactions and the diurnal cycle of low-level clouds and fog [J]. J Hydrometeor, 2017, 18(5): 1513-1533.
[38] MÜLLER M D, MASBOU M, BOTT A. 2010. Three-dimensional fog forecasting in complex terrain [J]. Quart J Roy Meteor Soc, 136(653): 2189-2202.
[39] CUXART J, JIMéNEZ M A. Deep radiation fog in a wide closed valley: Study by numerical modeling and remote sensing [J]. Pure Appl Geophys, 2011, 169(5-6): 911-926.
[40] National Oceanic and Atmospheric Administration (NOAA). Surface weather observations and reports [R] //Federal meteorological handbook. Silver Spring, 1995: 94.
[41] TAYLOR G I. Eddy motion in the atmosphere [J]. Philos Trans Roy Soc London, 1915, 215A: 1-26.
[42] PAGOWSKI M, GULTEPE I, KING P. Analysis and modeling of an extremely dense fog event in southern Ontario [J]. J Appl Meteor, 2004, 43(1): 3-16.
[43] SKAMAROCK W C. A description of the advanced research WRF [J]. NCAR Technical, 2008, 113: 7-25.
[44] ZHANG Chao-lin, MIAO Shi-guang, LI Qing-chun, et al. Impacts of fine-resolution land use information of Beijing on a summer severe rainfall simulation [J]. Chin J Geophys, 2007, 50(5): 1372-1382 (in Chinese).
[45] HONG S Y, LIM J O J. The WRF single-moment 6-class microphysics scheme (WSM6) [J]. J Korean Meteor Soc, 2006, 42(2): 129-151.
[46] MLAWER E J, TAUBMAN S J, BROWN P D, et al. Radiative transfer for inhomogeneous atmospheres: RRTM, a validated correlated-k model for the longwave [J]. J Geophys Res Atmos, 1997, 102 (D14): 16663-16682.
[47] DUDHIA J. Numerical study of convection observed during the winter monsoon experiment using a mesoscale two dimensional model [J]. J Atmos Sci, 1989, 46(20): 3077-3107.
[48] SUKORIANSKY S, GALPERIN B, PEROV V. Application of a new spectral theory of stably stratified turbulence to the atmospheric boundary layer over sea

ice [J]. Bound-Layer Meteor, 2005, 117(2): 231-257.
[49] KAIN J S. The Kain-Fritsch convective parameterization: An update [J]. J Appl Meteor, 2004, 43(1): 170-181.
[50] KUNKEL B A. Parameterization of droplet terminal velocity and extinction coefficient in fog models [J]. J Appl Meteor, 1984, 23(1): 34-41.
[51] STOELINGA M T, WARNER T T. Nonhydrostatic, mesobeta-scale model simulations of cloud ceiling and visibility for an East Coast winter precipitation event [J]. J Appl Meteor, 1999, 38(4): 385-404.
[52] FU G, GUO J, XIE S P, et al. Analysis and high-resolution modeling of a dense sea fog event over the Yellow Sea [J]. Atmos Res, 2006, 81(4): 293-303.
[53] LI Xiao-na, HUANG Jian, SHEN Shuang-he, et al. Evolution of liquid water content in a sea fog controlled by a high-pressure pattern [J]. J Trop Meteor, 2010, 16 (4): 409-416.
[54] ZHOU B, FERRIER B S. Asymptotic analysis of equilibrium in radiation fog [J]. J Appl Meteor Climatol, 2008, 47(6): 1704-1722.

Citation: ZHANG Fu-ying, LIU Hai-wen, ZHU Yu-xiang, et al. The impact of mountain to basin winds on the diurnal variation in fog over the Sichuan Basin, China [J]. J Trop Meteor, 2019, 25(2): 257-268.